

Pure Spin Current Injection in Hydrogenated Graphene Structures

Reinaldo Zapata-Peña¹, Bernardo S. Mendoza¹, Anatoli I. Shkrebtii²

¹*Centro de Investigaciones en Óptica, León, Guanajuato 37150, México and*

²*University of Ontario, Institute of Technology, Oshawa, ON, L1H 7L7, Canada*

(Dated: May 31, 2017)

Lorem ipsum dolor sit amet, consectetur adipiscing elit. Etiam lobortis facilisis sem. Nullam nec mi et neque pharetra sollicitudin. Praesent imperdiet mi nec ante. Donec ullamcorper, felis non sodales commodo, lectus velit ultrices augue, a dignissim nibh lectus placerat pede. Vivamus nunc nunc, molestie ut, ultricies vel, semper in, velit. Ut porttitor. Praesent in sapien. Lorem ipsum dolor sit amet, consectetur adipiscing elit. Duis fringilla tristique neque. Sed interdum libero ut metus. Pellentesque placerat. Nam rutrum augue a leo. Morbi sed elit sit amet ante lobortis sollicitudin. Praesent blandit blandit mauris. Praesent lectus tellus, aliquet aliquam, luctus a, egestas a, turpis. Mauris lacinia lorem sit amet ipsum. Nunc quis urna dictum turpis accumsan semper.

I. INTRODUCTION

Lorem ipsum dolor sit amet, consectetur adipiscing elit. Etiam lobortis facilisis sem. Nullam nec mi et neque pharetra sollicitudin. Praesent imperdiet mi nec ante. Donec ullamcorper, felis non sodales commodo, lectus velit ultrices augue, a dignissim nibh lectus placerat pede. Vivamus nunc nunc, molestie ut, ultricies vel, semper in, velit. Ut porttitor. Praesent in sapien. Lorem ipsum dolor sit amet, consectetur adipiscing elit. Duis fringilla tristique neque. Sed interdum libero ut metus. Pellentesque placerat. Nam rutrum augue a leo. Morbi sed elit sit amet ante lobortis sollicitudin. Praesent blandit blandit mauris. Praesent lectus tellus, aliquet aliquam, luctus a, egestas a, turpis. Mauris lacinia lorem sit amet ipsum. Nunc quis urna dictum turpis accumsan semper. Lorem ipsum dolor sit amet, consectetur adipiscing elit. Etiam lobortis facilisis sem. Nullam nec mi et neque pharetra sollicitudin. Praesent imperdiet mi nec ante. Donec ullamcorper, felis non sodales commodo, lectus velit ultrices augue, a dignissim nibh lectus placerat pede. Vivamus nunc nunc, molestie ut, ultricies vel, semper in, velit. Ut porttitor. Praesent in sapien. Lorem ipsum dolor sit amet, consectetur adipiscing elit. Duis fringilla tristique neque. Sed interdum libero ut metus. Pellentesque placerat. Nam rutrum augue a leo.

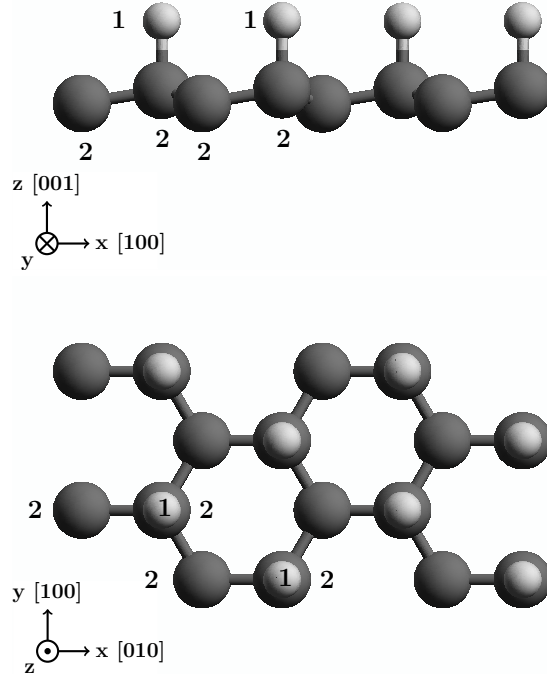


FIG. 1. Up structure `fig:up-struc`

Morbi sed elit sit amet ante lobortis sollicitudin. Praesent blandit blandit mauris. Praesent lectus tellus, aliquet aliquam, luctus a, egestas a, turpis. Mauris lacinia lorem sit amet ipsum. Nunc quis urna dictum turpis accumsan semper.

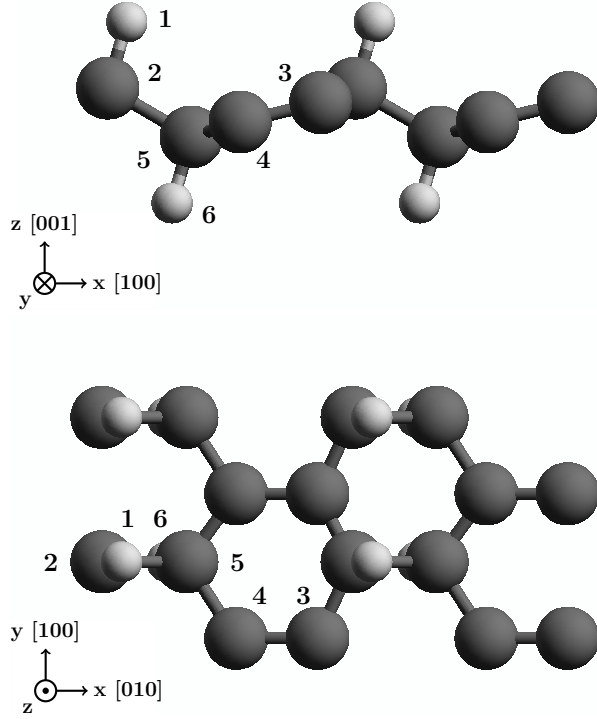


FIG. 2. Alt structure

Lorem ipsum dolor sit amet, consectetur adipiscing elit. Etiam lobortis facilisis sem. Nullam nec mi et neque pharetra sollicitudin. Praesent imperdiet mi nec ante. Donec ullamcorper, felis non sodales commodo, lectus velit ultrices augue, a dignissim nibh lectus placerat pede. Vivamus nunc nunc, molestie ut, ultricies vel, semper in, velit. Ut porttitor. Praesent in sapien. Lorem ipsum dolor sit amet, consectetur adipiscing elit. Duis fringilla tristique neque. Sed interdum libero ut metus. Pellentesque placerat. Nam rutrum augue a leo. Morbi sed elit sit amet

ante lobortis sollicitudin. Praesent blandit blandit mauris. Praesent lectus tellus, aliquet aliquam, luctus a, egestas a, turpis. Mauris lacinia lorem sit amet ipsum. Nunc quis urna dictum turpis accumsan semper.

Lorem ipsum dolor sit amet, consectetur adipiscing elit. Etiam lobortis facilisis sem. Nullam nec mi et neque pharetra sollicitudin. Praesent imperdiet mi nec ante. Donec ullamcorper, felis non sodales commodo, lectus velit ultrices augue, a dignissim nibh lectus placerat pede. Vivamus nunc nunc, molestie ut, ultricies vel, semper in, velit. Ut porttitor. Praesent in sapien. Lorem ipsum dolor sit amet, consectetur adipiscing elit. Duis fringilla tristique neque. Sed interdum libero ut metus. Pellentesque placerat. Nam rutrum augue a leo. Morbi sed elit sit amet ante lobortis sollicitudin. Praesent blandit blandit mauris. Praesent lectus tellus, aliquet aliquam, luctus a, egestas a, turpis. Mauris lacinia lorem sit amet ipsum. Nunc quis urna dictum turpis accumsan semper.

II. THEORY

sec:theory

A. Pure spin velocity

sec:theory-pure_spin_current

The spin density injection current $\dot{K}^{ab}(\omega)$, where the roman superscripts denote Cartesian components corresponding a to the spin velocity direction and b to the spin polarization direction, can be written in terms of a material response pseudotensor $\mu^{abcd}(\omega)$ as

$$\dot{K}^{ab}(\omega) = \mu^{abcd}(\omega) E^c(\omega) E^{d*}(\omega)$$

where the pseudotensor is given by¹

$$\mu^{abcd}(\omega) = \frac{\pi e^2}{\hbar^2} \int \frac{d^3 K}{8\pi^3} \sum'_{vcc'} \text{Re} \left[K_{cc'}^{ab} \left(r_{vc}^c r_{cv}^d + (c \leftrightarrow d) \right) \right] \delta(\omega - \omega_{cv}) \quad \text{eq:mu (1)}$$

where $K_{mn}^{ab}(\mathbf{k}) = \sum_{\ell} v_{nl}^a(\mathbf{k}) S_{lm}^b(\mathbf{k})$ are the spin current matrix elements that, using time reversal invariance, satisfy the relation $K_{nm}^{ab}(-\mathbf{k}) =$

$K^{ab*}(\mathbf{k})$. The ' in the sum means that c and c' are quasi degenerate states and the sum only covers these states and since μ is real we have

that $\mu^{abcd}(\omega) = \mu^{abdc}(\omega)$. Now we define the spin velocity, $\mathcal{V}^{ab}(\omega, \alpha)$ as the speed at which the

spin polarized in the b direction moves along the a direction when a normal incident beam reaches the xy plane with a polarization angle α as

$$\begin{aligned} \mathcal{V}^{ab}(\omega, \alpha) &= \frac{2}{\hbar} \frac{\mu^{abxx}(\omega)E^2(\omega)\cos^2(\alpha) + \mu^{abyy}(\omega)E^2(\omega)\sin^2(\alpha) + 2\mu^{abxy}(\omega)E^2(\omega)\cos(\alpha)\sin(\alpha)}{\xi^{xx}(\omega)E^2(\omega)\cos^2(\alpha) + \xi^{yy}(\omega)E^2(\omega)\sin^2(\alpha)}, \\ &= \frac{2}{\hbar} \frac{\mu^{abxx}(\omega)\cos^2(\alpha) + \mu^{abyy}(\omega)\sin^2(\alpha) + \mu^{abxy}(\omega)\sin(2\alpha)}{\xi^{xx}(\omega)\cos^2(\alpha) + \xi^{yy}(\omega)\sin^2(\alpha)}, \end{aligned} \quad \text{eq: vab} \quad (2)$$

where $\xi^{aa}(\omega)$ are the carrier generation rate tensor components². For an angle $\alpha = \frac{\pi}{4}$ this expression can be reduced to

$$\mathcal{V}^{ab}(\omega) = \frac{2}{\hbar} \frac{\mu^{abxx}(\omega) + \mu^{abyy}(\omega) + 2\mu^{abxy}(\omega)}{\xi^{xx}(\omega) + \xi^{yy}(\omega)}.$$

B. Fixing spin

sec:theory-fixspin

Considering that we have 2D structures, one of the options to analyze the spin velocity (Eq. (2)) is fixing the spin parallel to the surface of the structure in the x or y directions or perpendicularly to it in the z direction. We define the magnitude of the spin velocity with spin polarization along the b Cartesian coordinate as

$$|\mathcal{V}_{\sigma^b}(\omega, \alpha)| = \sqrt{[\mathcal{V}^{ax}(\omega, \alpha)]^2 + [\mathcal{V}^{ay}(\omega, \alpha)]^2} \quad \text{eq: vs-mag} \quad (3)$$

and the angle at which the spin velocity is directed on the xy plane as

$$\gamma_b(\omega, \alpha) = \tan^{-1} \left(\frac{\mathcal{V}^{ay}(\omega, \alpha)}{\mathcal{V}^{ax}(\omega, \alpha)} \right), \quad \text{eq: gamma-ang} \quad (4)$$

where the angle is measured in the counter-clockwise direction from the positive x Cartesian coordinate. We also define two special angles

$$\gamma_{b\parallel}(\omega, \alpha) = \alpha, \quad \text{eq: gamma-par} \quad (5)$$

$$\gamma_{b\perp}(\omega, \alpha) = \alpha \pm 90^\circ. \quad \text{eq: gamma-perp} \quad (6)$$

The first corresponds to the case when the spin velocity is directed, on the xy plane in the same direction of the polarization angle of the incoming beam; the second one corresponds to the case when the spin velocity is directed perpendicularly respect to the polarization angle of the incoming beam.

C. Fixing velocity.

sec:theory-fixvel

Another possibility to analyze the Eq. (2) is fixing the velocity on the xy plane along x or y Cartesian coordinate and then define the magnitude of the spin velocity directed along the a direction as

$$|\mathcal{V}^a(\omega, \alpha)| = \sqrt{[\mathcal{V}^{ax}(\omega, \alpha)]^2 + [\mathcal{V}^{ay}(\omega, \alpha)]^2 + [\mathcal{V}^{az}(\omega, \alpha)]^2}, \quad \text{eq: vv-mag} \quad (7)$$

Then, the spin direction depends of the x , y , and z components of the previous equation and so we define the spin orientation polar and azimuthal angles as

$$\theta_a(\omega, \alpha) = \cos^{-1} \left(\frac{\mathcal{V}^{az}(\omega, \alpha)}{|\mathcal{V}^a(\omega, \alpha)|} \right), \quad 0 \leq \theta \leq \pi, \quad \text{eq: polar-ang} \quad (8)$$

$$\varphi_a(\omega, \alpha) = \tan^{-1} \left(\frac{\mathcal{V}^{ay}(\omega, \alpha)}{\mathcal{V}^{ax}(\omega, \alpha)} \right), \quad 0 \leq \varphi \leq 2\pi. \quad \text{eq: azimuthal-ang} \quad (9)$$

where $\theta_a(\omega, \alpha)$ is measured from the positive to the negative z Cartesian coordinate and $\varphi_a(\omega, \alpha)$ is measured on the xy plane in the counter-clockwise direction from the positive x Cartesian coordinate.

D. Layer-by-layer analysis.

sec:theory-layer

For a layered system we have that the total contribution of Eqns. (3) and (7) is given² by

Layer No.	Atom type	Position [Å]		
		x	y	z
1	H	-0.61516	-1.77416	0.73196
1	H	0.61518	0.35514	0.73175
2	C	-0.61516	-1.77264	-0.49138
2	C	-0.61516	-0.35600	-0.72316
2	C	0.61516	0.35763	-0.49087

TABLE I. Unit cell of *up* structure. Layer division, atom types and positions for the *up* structure. The structure unit cell was divided in two layers corresponding to hydrogen and carbon atoms. The corresponding layer atom position is depicted in Fig. 1 with the corresponding number of layer.

Layer No.	Atom type	Position [Å]		
		x	y	z
1	H	-0.61516	-1.42140	1.47237
2	C	-0.61516	-1.73300	0.39631
3	C	0.61516	1.73300	0.15807
4	C	0.61516	0.42201	-0.15814
5	C	-0.61516	-0.37396	-0.39632
6	H	-0.61516	-0.68566	-1.47237

TABLE II. Unit cell of *alt* structure. Layer division, atom types and positions for the *alt* structure. The structure unit cell was divided in six layers corresponding each one to atoms in different z positions. The corresponding layer atom position is depicted in Fig. 2 with the corresponding number of layer.

$$|\mathcal{V}_{\sigma^b}(\omega, \alpha)| = \ell_{\text{eff}} \sum_{\ell=1}^{N_{\text{eff}}} |\mathcal{V}_{\sigma^b}(\ell|\omega, \alpha)| \quad \text{eq:vs-layer} \quad (10)$$

$$|\mathcal{V}^a(\omega, \alpha)| = \ell_{\text{eff}} \sum_{\ell=1}^{N_{\text{eff}}} |\mathcal{V}^a(\ell|\omega, \alpha)| \quad \text{eq:vv-layer} \quad (11)$$

III. RESULTS

We preset the results for $|\mathcal{V}^a(\omega, \alpha)|$ and $|\mathcal{V}_{\sigma^b}(\omega, \alpha)|$ for the C_{16}H_8 -alt and C_{16}H_8 -up structures being both noncentrosymmetric semi-infinite 2D carbon systems with 50% hydrogenation in different arrangements. The *up* structure has hydrogen atoms only on the upper side of the carbon sheet while the *alt* structure has al-

ternating hydrogen atoms on the upper and bottom sides. We take the hexagonal carbon lattice to be on the xy plane for both structures, and the carbon-hydrogen bonds on the perpendicular xz plane, as depicted in Figs. 2 and 1 and the coordinates for the *up* and *alt* unit cells of the structures are presented in Tables I and II. In same tables we present the layer division needed to calculate the layer-by-layer contribution for the $|\mathcal{V}_{\sigma^b}(\omega, \alpha)|$ and $|\mathcal{V}^a(\omega, \alpha)|$ presented in Eqns. (10) and (11). The *up* structure was divided in two layers, the first comprised of the top hydrogen atoms denoted by the number 1 in Table I and in the Fig. 1 and the second comprised of carbon atoms and denoted by the number 2. The *alt* structure was divided in six layers denoted with numbers from 1 to 6 in Table II and in Fig. 2. The first and sixth layers correspond to hydrogen atoms in the top and bottom positions and from the second to the fifth correspond to carbon atoms placed in different positions.

We calculated the self-consistent ground state and the Kohn-Sham states using density functional theory in the local density approximation (DFT- LDA) with a planewave basis using the ABINIT code³. We used Hartwigsen-Goedecker-Hutter (HGH) relativistic separable dual-space Gaussian pseudopotentials⁴ including the spin-orbit interaction needed to calculate $\mu^{\text{abcd}}(\omega, \alpha)$ presented in Eq. (1). The convergence parameters for the calculations of our results corresponding to the *alt* and *up* structures are cutoff energies of 65 Ha and 40 Ha, respectively. The energy eigenvalues and matrix elements for the *up* and *alt* structures were calculated using 14452 \mathbf{k} points and 8452 \mathbf{k} points in the irreducible Brillouin zone (IBZ) resulting in LDA energy band gaps of 0.72 eV and 0.088 eV, respectively. We notice that within DFT, the LDA is only one of other possible methods that can be used to determine the electronic structure of materials. Recent investigations on graphene show some of the differences in calculated values from several of these methods^{5,6}. We note that the LDA is as good as these other approaches. It is also known that the DFT calculations predict a band gap for the material that differs from experiment. This can be corrected using other *ab initio* techniques, such as the GW approximation⁷, but this calcu-

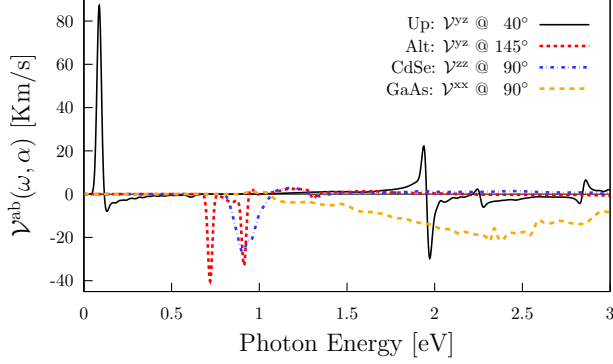


FIG. 3. Comparison of most intense responses of \mathcal{V}^{ab} for 2D *alt* and *up*, and bulk CdSe and GaAs structures and the corresponding polarization angles.

lation has a very high computational cost and is out of the scope in this paper. Even so, DFT still remains as an effective and useful tool for computing diverse properties derived from the electronic band structure.

A. Spin velocity

sec:res-spin_velocity

Using the Eq. (2), we calculated the $\mathcal{V}^{ab}(\omega, \alpha)$ response for the *up* and *alt* 2D structures and for the CdSe and GaAs bulk systems; the results are presented in Fig. 3. The angle α presented in the response of each structure is that for which the response is maximized in each case. From the figure we have that the onset of the response starts when the energy of the incoming beam is the same of the gap energy. The most intense response corresponds to the *up* structure centered at 0.088 eV corresponding to

Structure	Kind of system	Pol. Ang.	Energy [eV]	$\mathcal{V}^{ab}(\omega, \alpha)$ ab	[Km/s]
<i>up</i>	2D	40	0.09	yz	87.16
			1.94	yz	22.22
			1.97	yz	-29.70
<i>alt</i>	2D	145	0.72	yz	-40.21
			0.91	yz	-32.89
CdSe	bulk	90	0.91	zz	-26.87
GaAs	bulk	90	2.31	xx	-21.62

TABLE III. Comparison of the reported maxima values of \mathcal{V}^{ab} for different structures and the corresponding polarization angle α and energy values.

tab:vab-str-comp

the **Mid Infrared (MIR)** radiation and reaching a spin velocity of 87.2 Km/s. In the other hand, for an energy range from 0.66 eV to 3.0 eV, corresponding to energies of the **Near Infrared (NIR) to visible radiation**, all the four structures have contributions in the same order of magnitude. For this energy range the *up* structure has two peaks centered at 1.94 eV and 1.97 eV reaching spin velocities of 22.2 Km/s and -29.7 Km/s, respectively, and the *alt* structure has two peaks centered at 0.72 eV and 0.91 eV reaching spin velocities of -40.2 Km/s and -32.9 Km/s, respectively. Then, for the bulk structures we have that the CdSe has only one intense response centered at 0.91 eV reaching a spin velocity of -26.9 Km/s, and the GaAs structure has a large and almost planar zone where the response is held reaching the maximum for an incoming beam of energy of 2.31 eV and resulting in a spin velocity of -21.6 Km/s. A negative quantity in the spin velocity means a change in the spin polarization traveling in the opposite direction. In table III we present the comparison of this values for the 2D and bulk structures. We found that the most intense response for the spin velocity corresponds to the *up* structure being 3.25 times more intense than that of the CdSe and 4.03 times more intense than that of the GaAs bulk structures. Also, the *alt* structure has a response more intense than the bulk systems but being less intense than the corresponding to the *up* one.

B. Fixing spin

sec:res-fixspin

Using the Eq. (3), we calculated the $|\mathcal{V}_{\sigma^b}(\omega, \alpha)|$ response and made the analysis for the case when the spin is fixed in the z coordinate, directed perpendicularly to the surface of the *up* and *alt* structures. Also, using the Eq. (4), we determined the angle $\gamma_b(\omega, \alpha)$ where the spin-velocity is directed on the surface of the each structure.

Up structure

We first analyzed two energy ranges in Fig. 4 for the *up* structure, the first for an incoming energy beam from 0.0 eV to 0.2 eV (top panel) which include the THz and the Mid Infrared

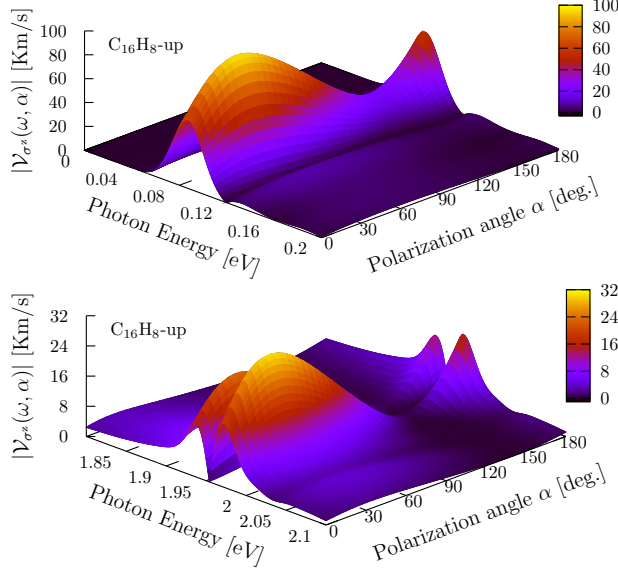


FIG. 4. $|\mathcal{V}_{\sigma^z}(\omega, \alpha)|$ response as a function of the photon energy and polarization angle α for the *up* structure for two energy ranges. The absolute maxima is located for an energy range from 0.08 eV to 0.10 eV, in the Far Infrared radiation range, and two local maxima from 1.90 eV to 1.93 eV and from 1.96 eV to 2.0 eV, in the visible radiation range, all for polarization angles between 25° and 50°. **fig:up-3d-vs**

(MIR) radiation, where the absolute maximum of the $|\mathcal{V}_{\sigma^z}(\omega, \alpha)|$ response is obtained, and the second for an energy range from 1.80 eV to 2.1 eV (bottom panel), corresponding to visible radiation, where two local maxima are found. Making the analysis, we obtained that the zone where the maximum response is held corresponds to a energy range of the incident beam from 0.084 eV to 0.093 eV and polarization angles α between 30° and 45°. Also the two local maxima are held for same beam polarization angles but for an energy range between 1.90 eV and 2.05 eV. In the top frames of top and bottom panels of Fig. 5 we present in solid lines the result of evaluate $|\mathcal{V}_{\sigma^z}(\omega, \alpha)|$, related to the left scale, fixing the energy of the incoming beam to 0.088 eV and 1.972 eV, respectively, values for which the response is maximized for the *up* structure. In the same panels and frames we present in dashed lines, related to the right scale, the corresponding velocity angle $\gamma_z(\omega, \alpha)$, and in the bottom frames of the panels we present the corresponding components $\mathcal{V}^{xz}(\omega, \alpha)$ and $\mathcal{V}^{yz}(\omega, \alpha)$. Also

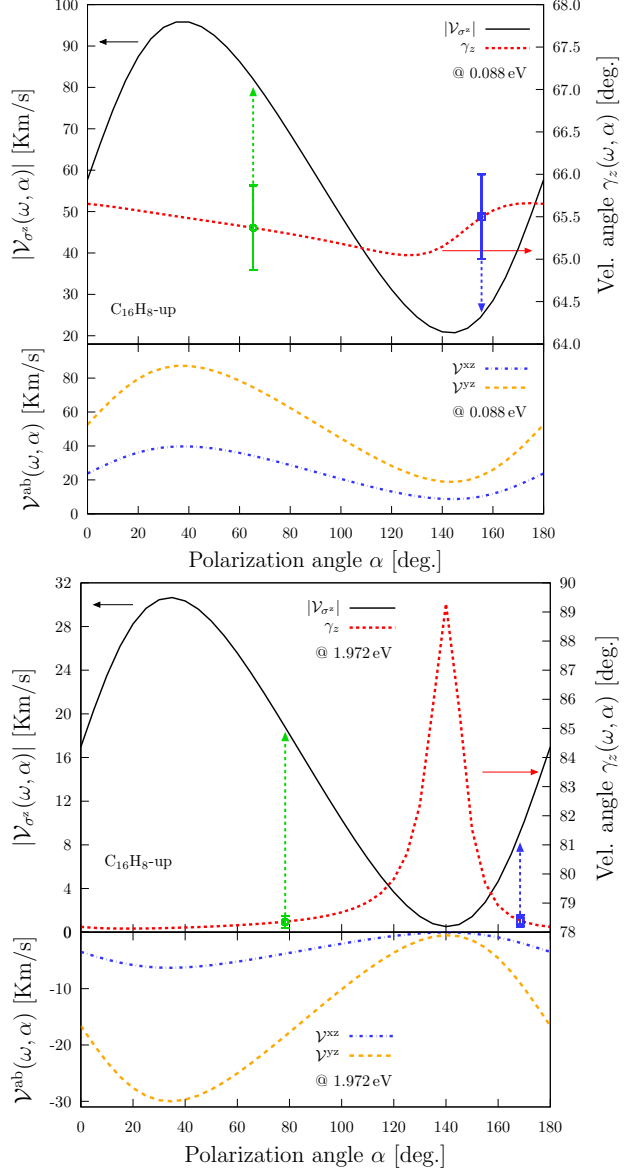


FIG. 5. Most intense response of $|\mathcal{V}_{\sigma^z}(\omega, \alpha)|$ (top frames, right scale of figs (a) and (b)), the corresponding velocity angle $\gamma_z(\omega, \alpha)$ (top frames, right scale), the collinear (circled box) and perpendicular (square box) angles, and the two components $\mathcal{V}^{xz}(\omega, \alpha)$ and $\mathcal{V}^{yz}(\omega, \alpha)$ (bottom frames) for the *up* structure fixing the energy to 0.088 eV and 1.972 eV, respectively, values for which the response is maximized for the *up* structure. **fig:up-vaz-rag**

we present two circled and square boxes indicating the values where the angles of the spin velocity are parallel (Eq. 5) and perpendicular (Eq. 6) and the arrows are directed to the value of the response corresponding to those angles. From top panels of Figs. 4 and 5 we have that the absolute maximum response for the *up* structure is obtained for an incom-

ing beam with energy of 0.088 eV and polarization angle $\alpha = 40^\circ$ resulting in a value of $|\mathcal{V}_{\sigma^z}(\omega, \alpha)| = 95.8 \text{ Km/s}$ coming from the contribution of the components $\mathcal{V}^{xz}(\omega, \alpha) = 39.8 \text{ Km/s}$ and $\mathcal{V}^{yz}(\omega, \alpha) = 87.2 \text{ Km/s}$ for the spin polarized in the z direction and having a velocity angle $\gamma_z(\omega, \alpha) = 65^\circ$ on the first Cartesian quadrant of the xy plane. From the top panel of Fig. 5 we have that the velocity angle is almost constant for all the polarization angle range having values of $\gamma_z(\omega, \alpha) = 65.5^\circ \pm 0.5^\circ$. In this panel the green circled box indicates the value for which the polarization angle and the response direction angle are collinear corresponding to $\gamma_{z\parallel}(\omega, \alpha) = 65.5^\circ$ and resulting in a value of the response of $|\mathcal{V}_{\sigma^z}(\omega, \alpha)| = 82.3 \text{ Km/s}$ indicated by the upward green arrow. Also the blue square box indicates the value for which the polarization angle and the response angle are perpendicular being $\alpha = 155.5^\circ$ and $\gamma_{z\perp}(\omega, \alpha) = 65.5^\circ$; for this angle the response has a value of $|\mathcal{V}_{\sigma^z}(\omega, \alpha)| = 24.8 \text{ Km/s}$ indicated by the blue downward arrow. Now, from bottom panels of Figs. 4 and 5 we have that the most intense local maximum of the response is obtained for an incoming beam with energy of 1.972 eV and same polarization angle $\alpha = 40^\circ$ resulting in a value of $|\mathcal{V}_{\sigma^z}(\omega, \alpha)| = 30.3 \text{ Km/s}$. This comes from a major contribution of the $\mathcal{V}^{yz}(\omega, \alpha)$ component being directed in a velocity angle $\gamma_z(\omega, \alpha) = 78^\circ$ on the first Cartesian Quadrant on the xy plane. Again from the bottom panel of Fig. 5 we found that the velocity angle is almost constant at 78° and has variations of 1° for polarization angles $0^\circ \leq \alpha \leq 100^\circ$. In this range the green circled box indicates the value for which the polarization angle and the response direction angle are collinear corresponding to $\gamma_{z\parallel}(\omega, \alpha) = 78.5^\circ$ and having a response value of $|\mathcal{V}_{\sigma^z}(\omega, \alpha)| = 23.5 \text{ Km/s}$ indicated with the green upward arrow. Finally, the blue square box indicates the value for which the polarization angle and the response angle are perpendicular being $\alpha = 168.5^\circ$ $\gamma_{z\perp}(\omega, \alpha) = 78.5^\circ$ and having a response $|\mathcal{V}_{\sigma^z}(\omega, \alpha)| = 9.0 \text{ Km/s}$ indicated with the blue upward arrow. We also made the analysis for the cases when the spin polarization is directed along the x and y Cartesian coordinates but we do not present here the corresponding plots. For those cases we have

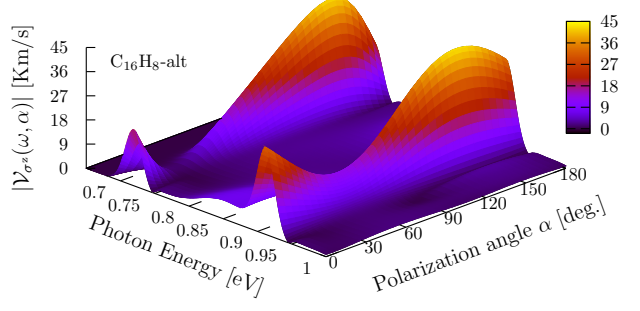


FIG. 6. $|\mathcal{V}_{\sigma^z}(\omega, \alpha)|$ response as a function of the photon energy and polarization angle α for the *alt* structure. The local and the absolute maxima are located in the energy ranges from 0.67 eV to 0.73 eV and from 0.90 eV to 0.93 eV, respectively, and both in the Near Infrared and for polarization angles between 120° and 150° . fig:alt-3d-vsbs

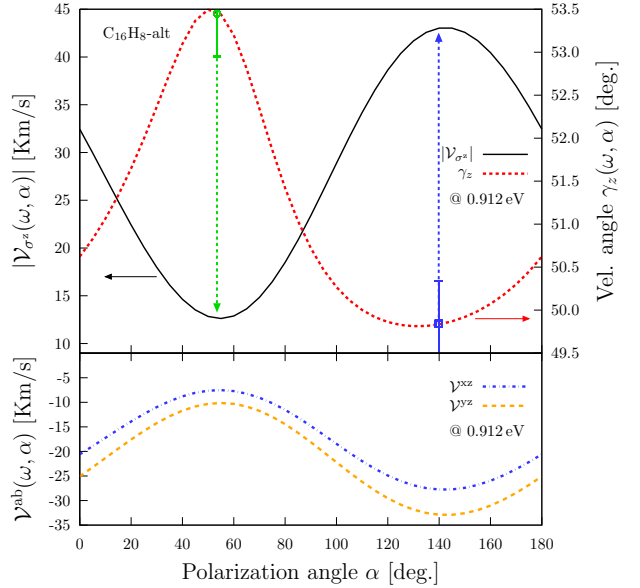


FIG. 7. Most intense response of $|\mathcal{V}_{\sigma^z}(\omega, \alpha)|$ (top frame, left scale) the corresponding velocity angle $\gamma_z(\omega)$ (top frame, right scale), the collinear (circled box) and perpendicular (square box) angles, and the two components $\mathcal{V}^{xz}(\omega)$ and $\mathcal{V}^{yz}(\omega)$ (bottom frame) for the *alt* structure fixing the energy to 0.912 eV. fig:alt-2d-vs-arg

that the absolute maxima responses are obtained for an energy of the incoming beam equal to 0.088 eV and polarization angle $\alpha = 40^\circ$ resulting in values of $|\mathcal{V}_{\sigma^x}(\omega, \alpha)| = 37.4 \text{ Km/s}$ and $|\mathcal{V}_{\sigma^y}(\omega, \alpha)| = 24.8 \text{ Km/s}$.

Alt structure

In Fig. 6 we analyzed the energy range for the incident beam from 0.6 eV to 1.0 eV, corre-

sponding to the NIR radiation, where the absolute maximum of $|\mathcal{V}_{\sigma^z}(\omega, \alpha)|$ response is obtained for the *alt* structure. From Figs. 6 and 7 we have that the absolute maximum response is obtained for an incoming beam with polarization angle $\alpha = 145^\circ$ reaching a velocity of $|\mathcal{V}_{\sigma^z}(\omega, \alpha)| = 43.0 \text{ Km/s}$ for the spin polarized in the z direction and resulting in a velocity angle $\gamma_z(\omega, \alpha) = 50^\circ$ on the first Cartesian Quadrant of the xy plane. Also, from the top frame of Fig. 7 we found that the velocity angle is centered at 51.5° having variations of $\pm 2^\circ$ for the polarization angle range $0^\circ \leq \alpha \leq 180^\circ$. As made in the previous analysis the circled box indicates the collinear angle (Eq. (5)) $\gamma_{z\parallel}(\omega, \alpha) = 53.5^\circ$ corresponding a value of $|\mathcal{V}_{\sigma^z}(\omega, \alpha)| = 12.7 \text{ Km/s}$; the blue square box indicates the perpendicular angles corresponding values $\alpha = 140^\circ$ and $\gamma_{z\perp}(\omega, \alpha) = 50^\circ$ with a value of $|\mathcal{V}_{\sigma^z}(\omega, \alpha)| = 43 \text{ Km/s}$. Again, for the cases in which the spin polarization is parallel to the surface of the *alt* structure was calculated but the plots are not presented here. The absolute maxima for the cases when the spin polarization are directed in the x and y direction are obtained for an energy of the incoming beam equal to 0.912 eV and polarization angle $\alpha = 145^\circ$ resulting in values of $|\mathcal{V}_{\sigma^x}(\omega, \alpha)| = 27.1 \text{ Km/s}$ and $|\mathcal{V}_{\sigma^y}(\omega, \alpha)| = 33.2 \text{ Km/s}$.

C. Fixing velocity

sec:res-fixvel

Now, using the Eq. (7), we calculated the $|\mathcal{V}^a(\omega, \alpha)|$ response and made the analysis for the case when the velocity is fixed in the x and y direction over the surface of the *alt* and *up* structures. Also, using the Eqns. (8) and (9), we determined the polar $\theta_a(\omega, \alpha)$ and azimuthal $\varphi_a(\omega, \alpha)$ angles where the spin polarization is directed.

Up structure.

In top and bottom panels of Fig. 8 we present the $|\mathcal{V}^x(\omega, \alpha)|$ and $|\mathcal{V}^y(\omega, \alpha)|$ spectra resulting from evaluate the Eq. (7) in the energy range for the incoming beam from 0.00 eV to 0.16 eV for the *up* structure. From this figure we can see that for the zone between the energy range of 0.084 eV - 0.093 eV and polarization angles be-

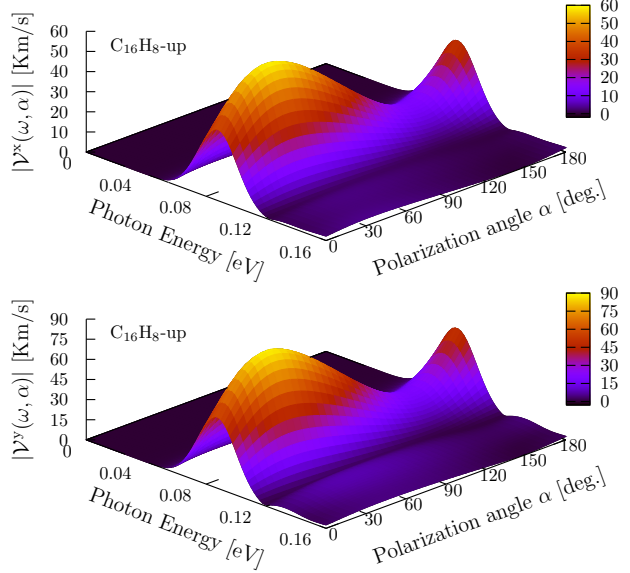


FIG. 8. $|\mathcal{V}^x(\omega, \alpha)|$ and $|\mathcal{V}^y(\omega, \alpha)|$ responses as a function of the photon energy and polarization angle α for the *up* structure. The absolute maxima of both are localized in the energy range from 0.08 eV to 0.10 eV , in the Far Infrared, and for polarization angles from 25° to 50° .
fig:up-3d-vva-1

tween 30° and 45° is the zone where the maximum response is held for both, $|\mathcal{V}^x(\omega, \alpha)|$ and $|\mathcal{V}^y(\omega, \alpha)|$.

In the top frames of top and bottom panels of Fig. 9 we present in solid lines the results of $|\mathcal{V}^x(\omega, \alpha)|$ and $|\mathcal{V}^y(\omega, \alpha)|$, related to the left scale, fixing the polarization angle to $\alpha = 40^\circ$ for which the response is maximized. In the same panels and frames we present in dashed lines the corresponding polar $\theta_a(\omega, \alpha)$ and azimuthal $\varphi_a(\omega, \alpha)$ spin polarization angles related to the right scale. Also, in the bottom frames of the panels we present the corresponding components $\mathcal{V}^{xx}(\omega, \alpha)$, $\mathcal{V}^{xy}(\omega, \alpha)$, $\mathcal{V}^{xz}(\omega, \alpha)$, and $\mathcal{V}^{yx}(\omega, \alpha)$, $\mathcal{V}^{yy}(\omega, \alpha)$, $\mathcal{V}^{yz}(\omega, \alpha)$. From the top panel of Fig. 9 we have that for an incoming beam with energy of 0.088 eV the three components have similar contributions with values of $\mathcal{V}^{xx}(\omega, \alpha) = -36.5 \text{ Km/s}$, $\mathcal{V}^{xy}(\omega, \alpha) = -23.2 \text{ Km/s}$, and $\mathcal{V}^{xz}(\omega, \alpha) = 39.8 \text{ Km/s}$ resulting in a response $|\mathcal{V}^x(\omega, \alpha)| = 58.7 \text{ Km/s}$ being this value the absolute maximum obtained when the spin-velocity is fixed in the x direction. To this value corresponds polar and azimuthal spin polarization angles of $\theta_x(\omega, \alpha) = 47$

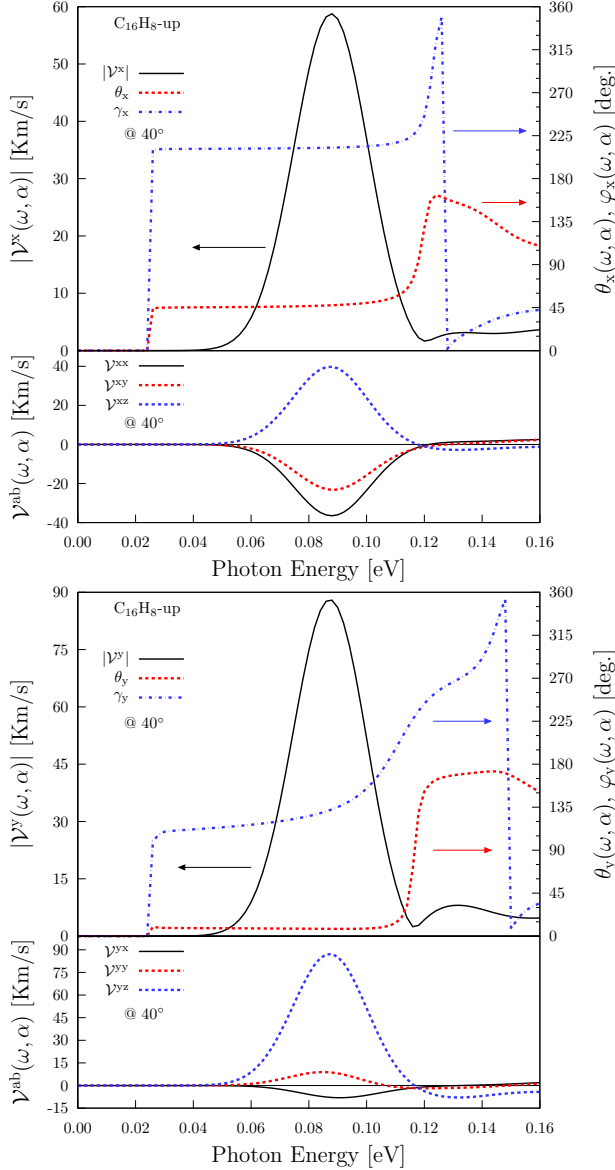


FIG. 9. Most intense response of $|\mathcal{V}^x(\omega, \alpha)|$ and $|\mathcal{V}^y(\omega, \alpha)|$ (top frames left scale of Figs. (a) and (b)), the corresponding polar φ and azimuthal θ angles (top frames right scale), and the corresponding three components (bottom frames) for the *up* structure fixing the polarization angle to $\alpha = 40^\circ$ to maximize the response.

fig:up-vab-comp-rtp-1

and $\varphi_x(\omega, \alpha) = 212$, respectively, being directed upward the third Cartesian quadrant of the *xy* plane. Also from this figure we have that those angles values are held for almost all the peak of the response having variations of $\pm 2^\circ$ each one. Now, from the bottom panel of Fig. 9 we have that the components have contributions of $\mathcal{V}^{yx}(\omega, \alpha) = -7.9 \text{ Km/s}$ $\mathcal{V}^{yy}(\omega, \alpha) = 8.6 \text{ Km/s}$,

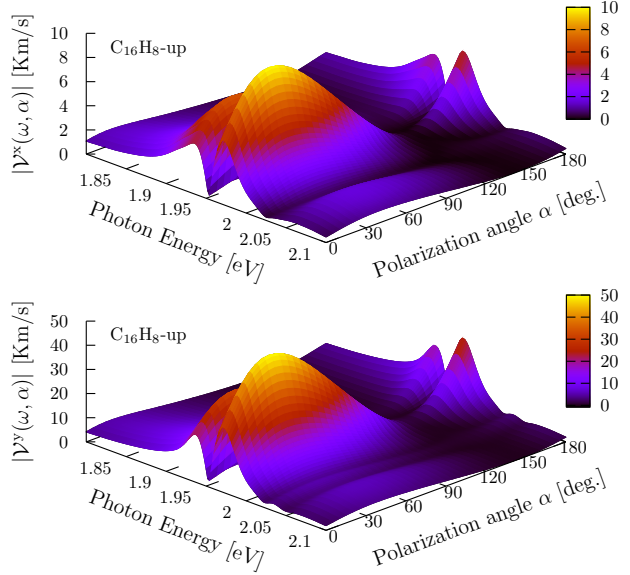


FIG. 10. $|\mathcal{V}^x(\omega, \alpha)|$ (top panel) and $|\mathcal{V}^y(\omega, \alpha)|$ (bottom panel) as a function of the photon energy and polarization angle α for the *up* structure. Two local maxima of both responses are localized in the energy range from 1.90 eV to 1.93 eV and from 1.96 eV to 2.0 eV, in the visible radiation range, and for polarization angles between 25° and 50°

fig:up-3d-vva-2

and $\mathcal{V}^{yz}(\omega, \alpha) = 87.2 \text{ Km/s}$ resulting in a response $|\mathcal{V}^y(\omega, \alpha)| = 87.9 \text{ Km/s}$. This value is the absolute maximum obtained when the spin-velocity is fixed in the *y* direction and is 1.5 times more intense than the maximum of $|\mathcal{V}^x(\omega, \alpha)|$ for this structure. To this absolute maximum corresponds spin polarization polar and azimuthal angles $\theta_y(\omega, \alpha) = 8^\circ$ and $\varphi_y(\omega, \alpha) = 133^\circ$ being directed the spin almost perpendicularly over the *xy* plane and localized on the first Cartesian quadrant. In a different way than in the $|\mathcal{V}^x(\omega, \alpha)|$ case for the $|\mathcal{V}^y(\omega, \alpha)|$ only the polar angle is held at 8° for the peak of the response having variations of $\pm 2^\circ$ but the azimuthal angle changes from 99° to 176° having a value of 133° for the maximum. We also found that since the onset of the response till an energy for the incoming beam of 0.118 eV the components of both responses, have no change in the spin polarization-velocity direction. Finally, after this last energy value the responses go to zero. Also there is another energy range of interest for an incoming energy beam from 1.80 eV to 2.10 eV, corresponding to visible radiation, presented in

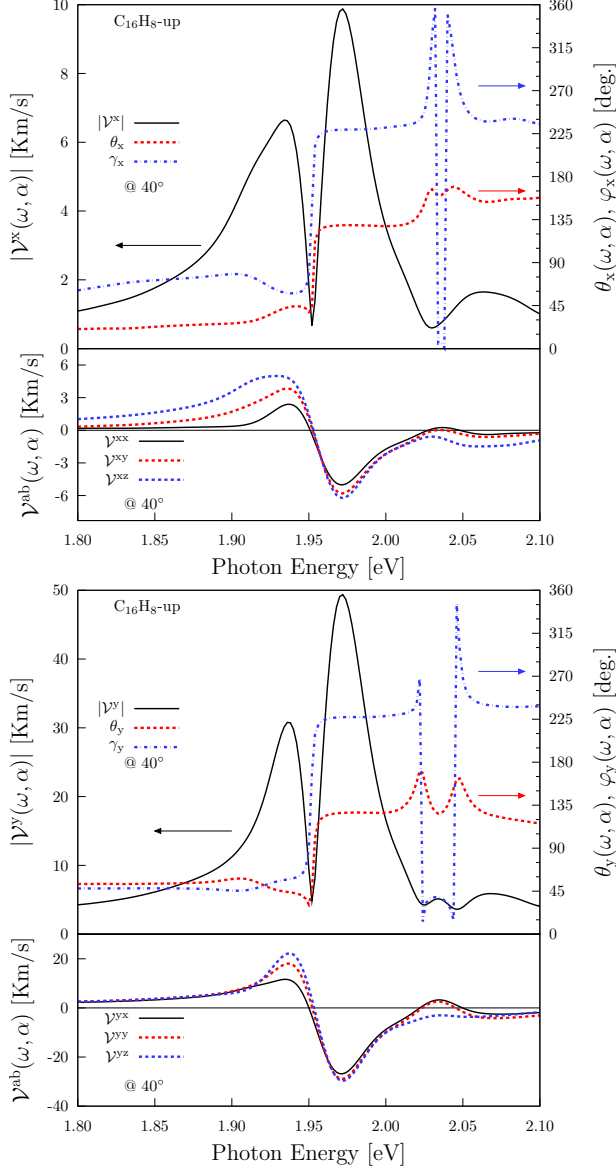


FIG. 11. Intense response of $|\mathcal{V}^x(\omega, \alpha)|$ and $|\mathcal{V}^y(\omega, \alpha)|$ (top frames left scale of Figs. (a) and (b)), the corresponding polar φ and azimuthal θ angles (top frames right scale), and the corresponding three components (bottom frames) for the *up* structure fixing the polarization angle to $\alpha = 40^\circ$ to maximize the response.

Fig. 10 where two local of both responses are obtained for the *up* structure for energies of 1.934 eV and 1.972 eV fixing again the polarization angle to 40° . We found that for both cases the components have similar contributions for each response and for 1.934 eV result in values of $|\mathcal{V}^x(\omega, \alpha)| = 6.6$ Km/s for the spin velocity moving along the *x* direction with polar and azimuthal spin polarization angles $\theta_x(\omega, \alpha) = 42^\circ$

and $\varphi_x(\omega, \alpha) = 59^\circ$ being the spin directed over the first Cartesian quadrant of the *xy* plane; for the spin moving along the *y* direction we have a response $|\mathcal{V}^y(\omega, \alpha)| = 28.7$ Km/s with polar and azimuthal spin polarization angles $\theta_y(\omega, \alpha) = 45^\circ$ and $\varphi_y(\omega, \alpha) = 56^\circ$ being the spin directed over the first Cartesian quadrant of the *xy* plane. Alike, for an incoming energy beam of 1.972 eV we found the second and more intense local maxima for which all the components have similar contributions for both responses. This result in values of $|\mathcal{V}^x(\omega, \alpha)| = 9.9$ Km/s and $|\mathcal{V}^y(\omega, \alpha)| = 49.4$ Km/s with spin polarization angles $\theta_x(\omega, \alpha) = 129^\circ$, $\varphi_x(\omega, \alpha) = 229^\circ$, $\theta_y(\omega, \alpha) = 127^\circ$ and $\varphi_y(\omega, \alpha) = 227^\circ$ being the spin directed downward the third Cartesian quadrant of the *xy* plane when it moves in the *x* direction and downward the third Cartesian quadrant when it moves along the *y* direction. Also all the components of the responses keep the spin polarization positive till an energy of the incoming beam equal to 1.954 eV when the spin polarization and current changes the direction. After an energy of 2.05 eV both responses goes to zero.

Alt structure.

For the *alt* structure we analyzed the energy range from 0.6 eV to 1.0 eV in Fig. 12, corresponding to the NIR radiation, where we found a local maxima and the most intense responses for $|\mathcal{V}^x(\omega, \alpha)|$ and $|\mathcal{V}^y(\omega, \alpha)|$. From this figure we can see that for the zone between the energy range of 0.90 eV-0.93 eV and polarization angles between 120° and 150° is the zone where the maximum for both responses is held. In the top frames of top and bottom panels of Fig. 13 we present the spectra of $|\mathcal{V}^x(\omega, \alpha)|$ and $|\mathcal{V}^y(\omega, \alpha)|$ fixing the polarization angle to $\alpha = 145^\circ$ for which the response is maximized and its corresponding polar and azimuthal angles; in the bottom frames of same panels we present the corresponding three components $\mathcal{V}^{xx}(\omega, \alpha)$, $\mathcal{V}^{xy}(\omega, \alpha)$, $\mathcal{V}^{xz}(\omega, \alpha)$, $\mathcal{V}^{yx}(\omega, \alpha)$, $\mathcal{V}^{yy}(\omega, \alpha)$ and $\mathcal{V}^{yz}(\omega, \alpha)$. Making the analysis when the energy of the incoming beam is 0.720 eV we have similar contributions from the components when the spin velocity is along the *x* direction and a major contribution from $\mathcal{V}^{yz}(\omega, \alpha)$ when the spin velocity is directed along *y* Cartesian axis.

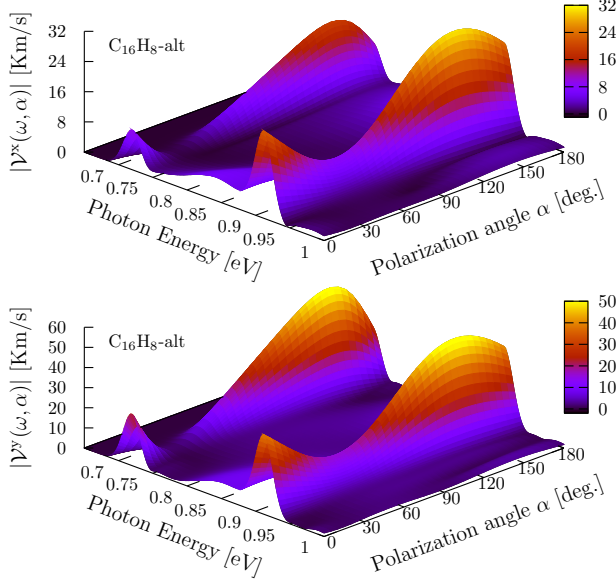


FIG. 12. $|V^x(\omega, \alpha)|$ (top panel) and $|V^y(\omega, \alpha)|$ (bottom panel) as a function of the photon energy and polarization angle α for the *alt* structure. The local and the absolute maxima are located in the energy ranges from 0.67 eV to 0.73 eV and from 0.90 eV to 0.93 eV, respectively, and both in the Near Infrared and for polarization angles between 120° and 150° .

This result in values of $|V^x(\omega, \alpha)| = 19.4 \text{ Km/s}$ and $|V^y(\omega, \alpha)| = 51.9 \text{ Km/s}$ with spin polarization angles $\theta_x(\omega, \alpha) = 46^\circ$, $\varphi_x(\omega, \alpha) = 41^\circ$, $\theta_y(\omega, \alpha) = 141^\circ$ and $\varphi_y(\omega, \alpha) = 222^\circ$ being the spin polarization directed over the first Cartesian quadrant of the xy plane when the spin velocity is directed along x and directed downward the third Cartesian quadrant when the spin velocity is directed along y . Then, for an energy of 0.912 eV we have values of $|V^x(\omega, \alpha)| = 30.9 \text{ Km/s}$ and $|V^y(\omega, \alpha)| = 52.3 \text{ Km/s}$. The first of them have a major contribution from the $V^{xz}(\omega, \alpha)$ component and the second one having similar contributions from all of three components. They result in polar and azimuthal angles $\theta_x(\omega, \alpha) = 154^\circ$, $\varphi_x(\omega, \alpha) = 290^\circ$, $\theta_y(\omega, \alpha) = 129^\circ$ and $\varphi_y(\omega, \alpha) = 229^\circ$ being the spin polarization directed downward the fourth Cartesian quadrant of the xy plane when the spin velocity is directed along x and downward the third Cartesian quadrant of the xy plane when the spin velocity is directed along y . Finally we have that the three components of $|V^y|$ are negative keeping the same spin polarization and velocity

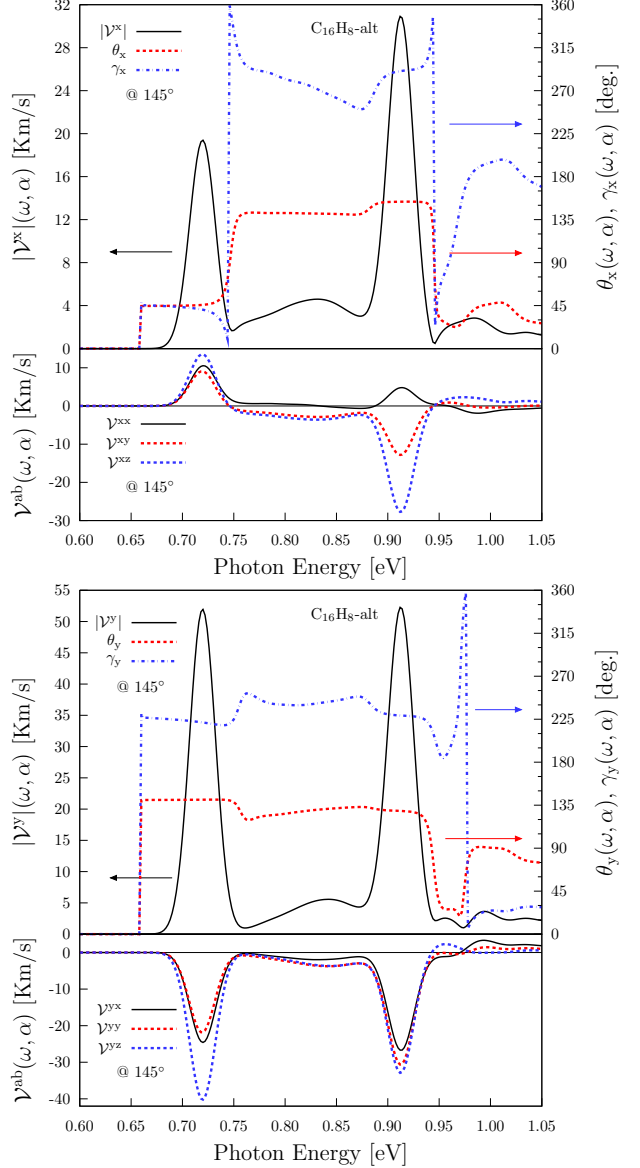


FIG. 13. Most intense response of $|V^x(\omega, \alpha)|$ and $|V^y(\omega, \alpha)|$ (top frames left scale of Figs. (a) and (b)), the corresponding polar φ and azimuthal θ angles (top frames right scale), and the corresponding three components (bottom frames) for the *alt* structure fixing the polarization angle to $\alpha = 145^\circ$ to maximize the response.

fig:alt-vab-comp-rtp

direction since the onset of the response to a energy of the incoming beam of 0.886 eV when the response decreases and goes to zero.

IV. LAYER-BY-LAYER ANALYSIS

sec:res-layer_by_layer_analysis

As mentioned before in in the beginning

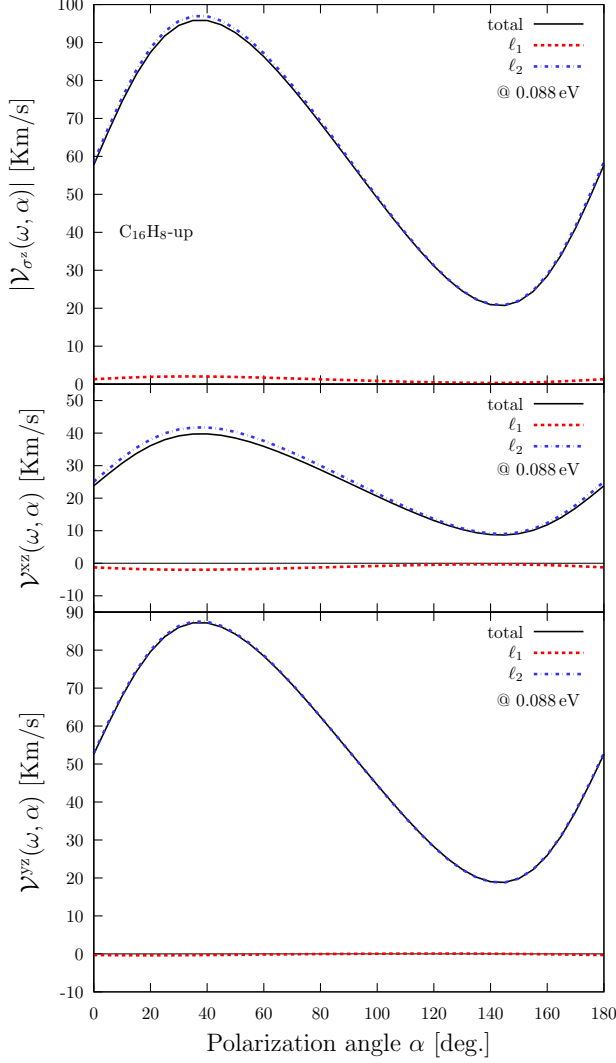


FIG. 14. Layer-by-layer contribution of the $|\mathcal{V}_{\sigma^z}(\omega, \alpha)|$ response (top frame) for the *up* structure as a function of the polarization angle α for the energy fixed to 0.088 eV for which the absolute maximum is obtained. The corresponding layered contributions for the $\mathcal{V}^{xz}(\omega, \alpha)$ and $\mathcal{V}^{yz}(\omega, \alpha)$ components are presented in the central and bottom frames.

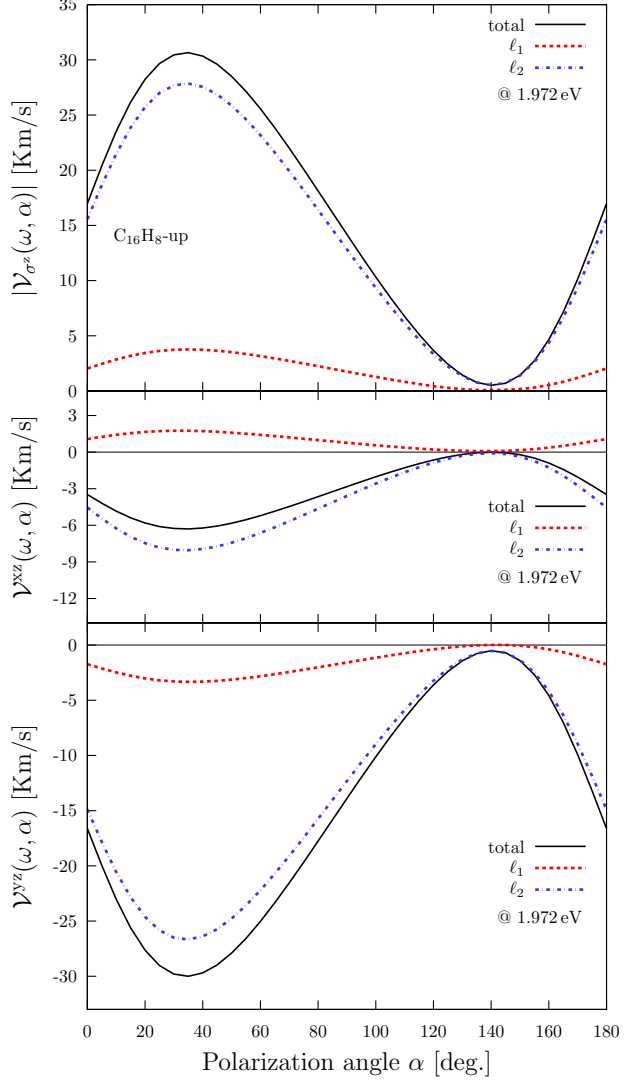


FIG. 15. Layer-by-layer contribution of the $|\mathcal{V}_{\sigma^z}(\omega, \alpha)|$ response (top frame) for the *up* structure as a function of the polarization angle α for the energy fixed to 1.972 eV for which a local maximum is obtained. The corresponding layered contributions for the $\mathcal{V}^{xz}(\omega, \alpha)$ and $\mathcal{V}^{yz}(\omega, \alpha)$ components are presented in the central and bottom frames.

of this section the *up* and *alt* structures presented here was divided into layers to analyze the layer-by-layer contribution for $|\mathcal{V}_{\sigma^z}(\omega, \alpha)|$ and $|\mathcal{V}^a(\omega, \alpha)|$. Here we present the decomposition only for $|\mathcal{V}_{\sigma^z}(\omega, \alpha)|$ and for the corresponding components of the *up* structure in Figs. 14 and 15 and for the *alt* structure in Fig. 16. The $|\mathcal{V}_{\sigma^z}(\omega, \alpha)|$ response presented in those figures is the same than the presented in top frames of Figs. 5 and 7 but now compared with the layered responses.

From the central and bottom frames of Fig. 14 we have that when the energy is fixed to 0.088 eV almost all the response of the $\mathcal{V}^{xz}(\omega, \alpha)$ component comes from the second layer comprised by carbon atoms having a minimal reduction produced by the hydrogen layer. Also, the $\mathcal{V}^{yz}(\omega, \alpha)$ response, presented in bottom frame of same figure, is produced only by the carbon layer. This result in a total response $|\mathcal{V}_{\sigma^z}(\omega, \alpha)| = 95.8 \text{ Km/s}$ coming from the carbon

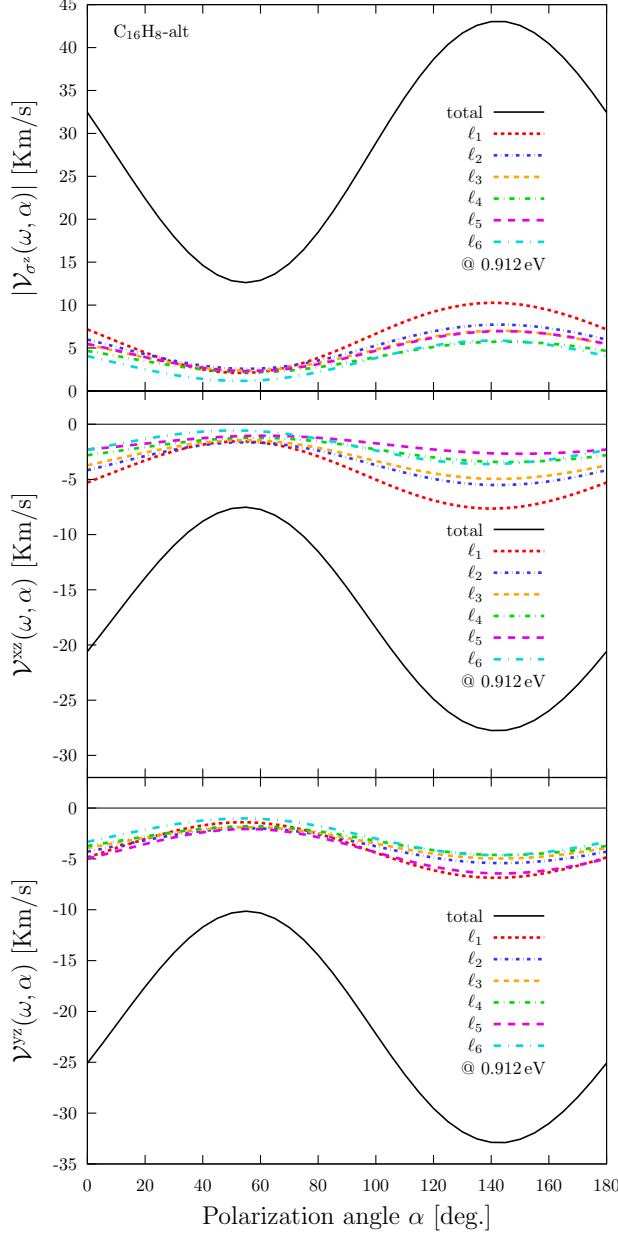


FIG. 16. Layer-by-layer contribution of the $|V_{\sigma z}(\omega, \alpha)|$ response (top frame) for the *alt* structure as a function of the polarization angle α for the energy fixed to 0.912 eV for which the absolute maximum is obtained. The corresponding layered contributions for the $V^{xz}(\omega, \alpha)$ and $V^{yz}(\omega, \alpha)$ components are presented in the central and bottom frames.

layer and being minimally reduced by the hydrogen layer as shown in the top frame of this figure. Now, for the same structure but now fixing the energy to 1.972 eV we have from the central frame of Fig. 15 that the carbon layer produces the response of the $V^{zx}(\omega, \alpha)$ component being decreased by the hydrogen layer. Opposite to that, in the bottom frame of same figure we obtained that the response of the carbon and hydrogen layer are not inverse and then contributing both to the total response of $V^{yz}(\omega, \alpha)$. Then, in the top frame of this figure we have that the major contribution to the $|V_{\sigma z}(\omega, \alpha)|$ comes from the carbon layer with but being in this case reinforced by the contribution of the hydrogen layer and resulting in a value of 30.3 Km/s. Finally, for the *alt* structure we have that the six layers contribute with similar magnitudes and reinforce the $V^{xz}(\omega, \alpha)$ and $V^{yz}(\omega, \alpha)$ components resulting in a total response $V^{xz}(\omega, \alpha) = 43$ Km/s.

- ¹ R. R. Bhat, F. Nastos, A. Najmaie, and J. Sipe, Physical review letters **94**, 096603 (2005).
- ² N. Arzate, R. A. Vázquez-Nava, and B. S. Mendoza, Phys. Rev. B **90**, 205310 (2014).
- ³ X. Gonze, B. Amadon, P.-M. Anglade, J.-M.

Beuken, F. Bottin, P. Boulanger, F. Bruneval, D. Caliste, R. Caracas, M. Côté, T. Deutsch, L. Genovese, P. Ghosez, M. Giantomassi, S. Goedecker, D. Hamann, P. Hermet, F. Jollet, G. Jomard, S. Leroux, M. Mancini, S. Mazevet,

- M. Oliveira, G. Onida, Y. Pouillon, T. Rangel, G.-M. Rignanes, D. Sangalli, R. Shaltaf, M. Torrent, M. Verstraete, G. Zerah, and J. Zwanziger, *Comput. Phys. Commun.* **180**, 2582 (2009).
- ⁴ C. Hartwigsen, S. Goedecker, and J. Hutter, *Phys. Rev. B* **58**, 3641 (1998).
- ⁵ P. Karamanis, N. Otero, and C. Pouchan, *J. Phys. Chem. C* **119**, 11872 (2015).
- ⁶ A. R. Botello-Méndez, S. M. Dubois, A. Lherbier, and J. C. Charlier, *Acc. Chem. Res.* **47**, 3292 (2014).
- ⁷ G. Onida, L. Reining, and A. Rubio, *Rev. Mod. Phys.* **74**, 601 (2002).

LastBibitem